

Final Year Research Project Report

ELECTENG 700A/B

Project #48: Sunlink II: Light-Based Wireless
Communication Using Sunlight

Department of Electrical and Electronics Engineering
University of Auckland, Auckland, New Zealand

Vivek Chauhan

October 19, 2025



ENGINEERING
DEPARTMENT OF ELECTRICAL,
COMPUTER, AND SOFTWARE ENGINEERING

Student ID: 675090288
Student Email: vcha949@aucklanduni.ac.nz
Submitted: 19 October 2025
Project Partner: Ryan Farrell
Supervisors: Prof. Talia Xu

Disclaimer- All these conference papers have been submitted as partial fulfilment for the project requirement for the BE(Hons) degree. Although they have been assessed, no errors or factual information have been corrected or checked.

Declaration

Student

I hereby declare that:

1. This report is the result of the final year project work carried out by my project partner (see cover page) and I under the guidance of our supervisor (see cover page) in the 2025 academic year at the Department of Electrical, Computer and Software Engineering, Faculty of Engineering, University of Auckland.
2. This report is not the outcome of work done previously.
3. This report is not the outcome of work done in collaboration, except that with a potential project sponsor (if any) as stated in the text.
4. This report is not the same as any report, thesis, conference article or journal paper, or any other publication or unpublished work in any format.

In the case of a continuing project, please state clearly what has been developed during the project and what was available from previous year(s):

Signature: U.Chauhan

Date: 18/10/2025

Abstract

This project investigates the feasibility of sunlight-based visible light communication (VLC) through the design and implementation of Sunlink II, a prototype system that integrates sun-tracking control with optical data transmission. The research aimed to develop a reliable, low-power communication platform capable of using direct sunlight as the carrier medium while maintaining alignment through active mechanical tracking.

The study combined simulation and prototyping to validate two primary subsystems: a motor-controlled sun-tracking unit and a frequency-modulated communication link. The tracking subsystem employed a dual-sensor grid of light-dependent resistors (LDRs) and photodiodes, interfaced with a PI-controlled NEMA 17 stepper motor to maintain maximum irradiance alignment. The communication subsystem implemented discrete frequency-shift keying (FSK) using an LCD optical modulator, evaluated under both ambient and dark-room conditions. Experimental testing confirmed consistent sensor symmetry, accurate motor response, and predictable optical attenuation with increasing distance.

Results demonstrated that sunlight can serve as a stable medium for short-range optical communication, with improved signal reliability under controlled tracking. However, the high power draw of the stepper motor highlighted a trade-off between tracking precision and overall energy efficiency. The findings establish a foundation for future development of energy-aware sunlight-based communication systems, including the use of curved sensor surfaces, lower-torque actuators, and adaptive tracking algorithms to achieve sustainable, self-powered operation.

Table of Contents

Declaration	i
Abstract	ii
Table of Contents	iv
List of Figures	v
List of Tables	vi
Glossary of Terms	vii
1. Introduction	1
2. Literature Review	2
2.1. Introduction to Wireless Communication in the IoT Era	2
2.2. Fundamentals of Visible Light Communication (VLC) and Its Evolution	3
2.3. Passive VLC Using Ambient Light	3
2.4. Passive VLC with Direct Sunlight: Toward Solar-Driven Communication	4
2.5. System Implementation: Backscatter and Retro-reflective Designs	5
2.6. Vision for Sun-tracking Light Communication Systems	6
2.7. Summary and Research Approach	6
3. Materials & Methods	8
3.1. Overview of Methodological Approach	8
3.2. System Architecture and Components	9
3.2.1. Hardware Components	9
3.2.2. Electrical Interfaces and Communication	10
3.3. Control and Tracking Methodology	10
3.3.1. Sensing and Feedback Mechanism	11
3.3.2. Controller Algorithm Design	11
3.3.3. Motor Actuation and PWM Control	11
3.3.4. Dynamic Modelling of the Tracking System	12
3.3.5. Controller Algorithm Workflow	12
3.3.6. Performance Summary	12
3.4. Communication Methodology	13
3.4.1. Modulation Scheme Application	13
3.5. Data Collection and Experimental Procedure	14
3.5.1. Simulation and Calibration	14
3.5.2. Tracking Subsystem Testing	14
3.5.3. Communication Subsystem Testing	15
3.5.4. Data logging and Processing	15
4. Results	16

4.1. Tracking Subsystem Results	16
4.1.1. Sensor Array Calibration & Testing Results	16
4.1.2. Voltage Response of LDR and Photo-diode Sensors	16
4.1.3. Motor measurements and System Performance	17
4.1.4. General Observations	18
4.2. Communication Results	18
4.2.1. Baseline Noise	18
4.2.2. Signal Amplitude and Distance Relationship	19
4.2.3. General Observations	20
5. Discussion	20
5.1. Interpretation of Results	20
5.2. Evaluation of Validity and Limitations	21
5.3. Contribution to Knowledge	21
5.4. Practical Implications and Real-World Relevance	22
6. Conclusion	23
7. Future Works	23
7.1. Sunlight Tracking Subsystem	24
7.2. Optical Communication Subsystem	24
7.3. System-Level Integration	24
Acknowledgements	25
Appendix A. LTSpice Simulation Circuit	27
Appendix B. Testing Setup Diagrams	28
Appendix C. Transmitted Oscilloscope Readings	29

List of Figures

2.1. Radio spectrum usage across New Zealand, showing extensive allocation across most frequency bands as of March 2024 [1].	2
3.1. Methodological flow diagram showing system development	9
3.2. Control loop architecture for dual-axis light tracking using PI feedback.	12
4.1. Incident illuminance versus sensor angle for four brightness settings (10–100%).	16
4.2. Sensor voltage (photo-diode and LDR) versus angle at four brightness levels.	17
4.3. Baseline oscilloscope noise signal under daylight (left) and dark-room (right) conditions.	19
4.4. Peak voltage (mV) at varying distances under daylight and dark-room conditions.	19
4.5. Peak voltage (mV) versus distance for daylight and dark-room conditions.	20
Appendix A.1. LTSpice Simulation Model of Azimuth Motor	27
Appendix B.1. Overall setup showing the Tracking Subsystem Testing	28
Appendix B.2. Overall setup showing the Communication Subsystem Testing	28
Appendix C.1. Transmitted and received FSK signals recorded across four distances under two lighting conditions.	29

List of Tables

3.1. Component voltage and power-rail configuration	10
3.2. Functional interface mapping to MCU connections	10
4.1. Measured and simulated electrical characteristics for the NEMA 17 azimuth motor.	18

Glossary of Terms

VLC	Visible Light Communication: A wireless communication technology that transmits data using modulated visible light rather than radio waves.
Li-Fi	Light Fidelity: A subset of VLC that uses LED lighting for bidirectional, high-speed communication similar to Wi-Fi.
IoT	Internet of Things: A network of interconnected devices that exchange data wirelessly to perform automated or intelligent functions.
LDR	Light Dependent Resistor: A sensor whose resistance decreases with increasing light intensity, used for light tracking and detection.
Photo-diode	A semiconductor device that converts incident light into electrical current, typically used for precise light measurement.
LC Shutter	Liquid Crystal Shutter: An optical device that modulates light transmission by altering the alignment of liquid crystals under an electric field.
PID / PI Control	Proportional-Integral(-Derivative) Control: A feedback control method used to minimise error between a measured signal and a desired set point.
Stepper Motor	A DC motor that moves in discrete steps, allowing for accurate positioning in tracking and control applications.
Optical Carrier	The light source or wavelength used to transmit data in an optical communication system.
Irradiance	The power of electromagnetic radiation per unit area received from a light source, measured in watts per square metre (W/m^2).
Sun Tracking	The process of continuously aligning a solar collector or sensor with the position of the sun to maximise light capture.
Backscatter Communication	A passive communication method that transmits data by reflecting or modulating existing light or RF signals.
SNR	Signal-to-Noise Ratio: A measure of signal quality relative to background noise, used to evaluate communication performance.

1. Introduction

Light-based wireless communication, as an emerging technology for efficient and high-speed data transmission, Utilises visible light as a communication carrier. Offering advantages such as high bandwidth, electromagnetic immunity, and compatibility with modern illumination systems. These characteristics make it an attractive alternative to conventional radio-frequency (RF) communication, particularly for Internet of Things (IoT) and low-power applications. Within the broader engineering context, this technology contributes to the growing need for sustainable and interference-free communication methods that reduce dependence on congested RF bands.

Despite the potential of Light-based wireless communication and VLC systems, their reliance on ambient or artificial light sources for testing and operation presents a significant challenge. While effective in controlled environments, these systems struggle in outdoor settings, where light intensity and direction fluctuate throughout the day. Artificial light sources often lack the irradiance and stability needed for long-range or consistent outdoor communication. This dependence hampers scalability and real-world applicability, highlighting the need for systems that can function effectively under natural light conditions.

The project addresses the problem of signal instability and limited scalability in ambient-light-based systems by investigating the use of direct sunlight as the primary means of communication. Sunlight provides a renewable and globally available illumination source that can support energy-autonomous and environmentally sustainable communication. However, problems occur with its intensity and orientation fluctuate due to daily solar movement and environmental conditions, leading to inconsistent transmission. To maintain reliable communication, the system must dynamically align with the sun's position and optimise light capture. This forms the basis of the central research problem: how to design a sunlight-based communication system that maintains stable and efficient data transmission while accounting for natural light variability and mechanical tracking constraints.

The project, Sunlink II: Light-Based Wireless Communication Using Sunlight, aims to design and implement a prototype system that integrates dynamic sun tracking with optical data transmission. The objectives of this work are to:

1. Review existing light-based wireless communication technologies and identify the limitations of ambient-light systems.
2. Establish performance criteria for sunlight-based communication and design a dual-axis sun-tracking subsystem capable of precise alignment.
3. Integrate the tracking subsystem with a light communication module that uses sunlight as the carrier signal.
4. Test the prototype under both indoor and outdoor conditions, analysing stability, energy efficiency, and signal quality.

Through this research, the project aims to contribute to the advancement of sustainable communication systems that leverage naturally available light sources while addressing real-world challenges in alignment, stability, and efficiency.

2. Literature Review

2.1. Introduction to Wireless Communication in the IoT Era

The Internet of Things (IoT) emerged as a transformative paradigm in the early 2010s[2], embedding connectivity into everyday objects to enable real-time data exchange across distributed systems. With billions of devices projected to come online in the coming years, the demand for reliable, scalable, and energy efficient wireless communication has intensified. Traditional radio frequency (RF) communication technologies, such as Wi-Fi, Bluetooth, and Zigbee, have served as the backbone of IoT networking. However, the exponential growth of connected devices has placed immense pressure on the RF spectrum, particularly within the overcrowded 2.4 GHz and 5 GHz bands [3]. Overcrowding is observable in national spectrum allocations, one source from New Zealand's 2024 Radio Spectrum Allocation Chart, maintained by the Ministry of Business, Innovation and Employment (MBIE), reveals that nearly the entire RF range—from Very Low Frequency (VLF) to Extremely High Frequency (EHF)—is already assigned for diverse applications such as broadcasting, mobile data, aviation, maritime services, satellite communication, and defence operations. Highly likely it will result in harder processes with implementation of new technologies in the future.

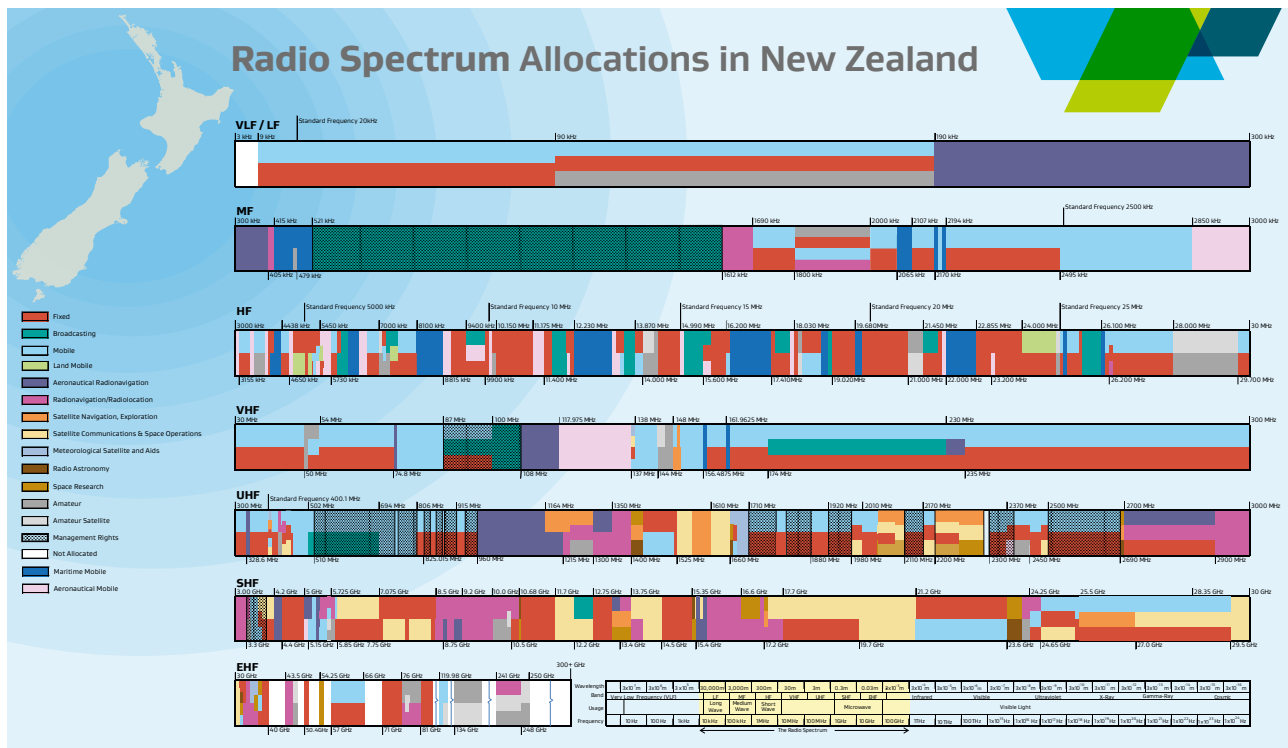


Figure 2.1: Radio spectrum usage across New Zealand, showing extensive allocation across most frequency bands as of March 2024 [1].

The growing constraints of the RF spectrum have led researchers to investigate alternative wireless communication methods. Visible Light Communication (VLC) has emerged as a promising candidate as a result, utilising the unlicensed and abundant visible spectrum to transmit data through light sources such as LEDs or natural sunlight. By operating outside conventional RF bands, VLC avoids spectral congestion while enabling dual-purpose functionality, such as combining illumination and data transmission. VLC aligns well with the energy constraints of IoT deployments, Especially in

passive VLC systems, where no active light emission is required from the transmitter side, communication can be achieved at dramatically reduced energy costs. Resulting in VLC being a candidate for the next generation of scalable, low-power IoT communication technologies.

Building upon this premise, exploring VLC as an emerging solution to RF congestion, It progresses from foundational VLC concepts to cutting-edge research in sunlight-based, passive communication systems—with a research focus specifically on the feasibility of real-time, sun-tracked, system-to-system communication.

2.2. Fundamentals of Visible Light Communication (VLC) and Its Evolution

Visible Light Communication (VLC) offers a promising alternative to RF-based wireless systems, particularly for energy-constrained and spectrum-scarce IoT deployments as mentioned before. Operating within the unlicensed 400–700 nm range, VLC enables data transmission through light intensity modulation. Typically using LEDs, allowing it to leverage existing lighting infrastructure for secure and energy-efficient communication [4]. Conventional VLC relies on actively modulated LEDs for downlink communication, which, while supporting high throughput, which inturn incurs considerable energy consumption. Presenting a barrier for ultra-low-power IoT applications, especially those relying on energy harvesting, which is problematic. Additionally, uplink communication in such systems often reintroduces RF components, undermining VLC's spectral benefits.

Addressing these limitations, passive VLC systems have emerged as a prominent field, these architectures eliminate the need for active emitters by modulating ambient or incident light using low-power optical components such as LCD shutters and/or retroreflectors. Significantly, reducing power consumption while supporting uplink communication in resource-constrained environments [5].

Recent efforts have introduced more systematic design approaches to passive VLC. A researcher, Ghiasi et al. present ChromaLux, a framework that leverages the transient, non-monotonic switching behaviour of liquid crystal (LC) cells to enhance modulation depth and speed [6]. By stacking multiple LC layers, ChromaLux broadens the modulation spectrum and achieves communication distances of up to 50 meters with error rates below 1% with ambient lighting conditions. Their design incorporates a novel duty-cycled modulation strategy and explores trade-offs between contrast and bandwidth using birefringence, [7], theory and the Michel-Lévy chart. Developing a shift from ad hoc designs toward structured, physics-informed architectures capable of supporting scalable and passive VLC systems for the next generation of IoT connectivity.

2.3. Passive VLC Using Ambient Light

Recent research has explored the feasibility of passive visible light communication (VLC) systems that rely on ambient light—such as sunlight, fluorescent bulbs, or uncontrolled LED fixtures—as the carrier medium for data transmission. Systems of such, are a particular interest in ultra-low-power IoT contexts where eliminating the need for modulated light sources can yield significant energy savings and system simplicity. One of the earliest and foundational works in this space is Passive Communication with Ambient Light by Wang et al. [4], proposing a communication system in which mobile objects modulate data using reflective surface patterns, without controlling the light

source itself. The authors demonstrated that by “wearing” sequences of high-contrast materials (e.g., aluminium tape and black paper), mobile devices could encode data that can be decoded by simple photo-diode-based receivers. The system however, was highly sensitive to environmental parameters such as distance, angle of incidence, light source intensity, and field-of-view (FoV).

To improve robustness under fluctuating lighting conditions, LuxLink proposed a frequency-based modulation (FSK) scheme for passive VLC using ambient light and LCD shutters [8]. Unlike earlier approaches that relied on pulse or amplitude modulation—both of which introduced flickering or instability, LuxLink demonstrated that FSK provided flicker-free and interference-resistant communication. The system achieved data rates of up to 80 bps at distances up to 60 meters outdoors, significantly outperforming earlier systems, while consuming minimal energy.

Edge-Light further expanded the ambient VLC design space by addressing a fundamental limitation in passive systems. The inability to communicate laterally (i.e. perpendicular to the direction of light propagation) [9], by integrating luminescent solar concentrators (LSCs) with LC shutters and colour sensors, the authors demonstrated lateral passive VLC links under both indoor and outdoor ambient lighting. Although limited by the low optical conversion efficiency (5%) of commercial LSCs, the system introduced a critical new capability of non-directional communication that does not require mechanical realignment.

These works together illustrate the growing maturity of ambient light-based passive VLC systems. However, a consistent theme across all three is the dependency on light variability. As Ullah et al. summarised, such systems ‘often face intensity variability and limited control over spectral consistency, which affects communication reliability’ [5]. These limitations have motivated recent research to explore direct sunlight as a more stable, high-intensity, and directionally consistent source for passive communication.

2.4. Passive VLC with Direct Sunlight: Toward Solar-Driven Communication

Many studies have explored the potential of direct sunlight as a communication medium in passive VLC systems. While, unlike ambient or artificial light, sunlight provides a high-intensity, spectrally broad, and globally available source, making it an appealing candidate for energy-efficient and scalable outdoor communication. This section continues by reviewing three systems, Sol-Fi, Sunlight-Duo, and SpectraLux, which all exemplify current approaches to leveraging sunlight for passive communication.

Sol-Fi introduces a system that combines sunlight collectors with passive modulators to deliver both natural illumination and data transmission indoors [10]. The system explores liquid crystal (LC) and digital micro-mirror device (DMD) modulators, offering a comparative analysis of their trade-offs in terms of modulation speed, area, power, and cost. Impressively, Sol-Fi also proposes a multibandmodulation approach, dividing the visible spectrum into separate bands to increase data throughput, achieving up to 80 kbps over 5 meters depending on configuration.

Sunlight-Duo extends passive VLC by using solar cells as dual-purpose receivers capable of simultaneous energy harvesting and data reception [11]. This system highlights the trade-off between maximising energy intake and decoding modulated data embedded in the same light stream. Through dynamic reconfiguration of solar cell parameters, the prototype maintains a bi-directional link up to

11 meters, supporting 1200 bps downlink and 800 bps uplink, powered by sunlight.

SpectraLux takes a different approach by shifting from spectrum-agnostic to spectrum-aware modulation using LC shutters and spectrometer-based receivers [12]. Rather than modulating light intensity alone, SpectraLux encodes data through spectral signatures generated by stacking and fine-tuning LC cells. This enables the use of multiple distinguishable symbols in the spectrum domain, increasing modulation quality even under the constraints of slow LC switching speeds.

Demonstrating growing maturity in sunlight-based passive VLC, each system addresses a unique aspect towards the area. Sol-Fi focuses on optical integration and multiband design, while Sunlight-Duo focuses on self-powered bidirectional links, and SpectraLux on advanced spectral modulation. These works collectively point toward the feasibility of robust and scalable communication systems that operate entirely on natural light.

2.5. System Implementation: Backscatter and Retro-reflective Designs

Passive visible light communication (VLC) relies on carefully engineered hardware and modulation schemes to enable energy-efficient communication without active emitters. Two implementations—PassiveVLC and RetroI2V, both demonstrate how backscatter communication can be achieved using retroreflectors and liquid crystal (LC) shutters, while being tailored to different application scenarios.

PassiveVLC presents a low-power, backscatter uplink system where a retroreflective fabric and a commercial LCD shutter are used to modulate incident light from overhead LEDs [13]. The system is powered entirely by harvested light through onboard solar cells, enabling fully battery-free operation. A key innovation is its trend-based modulation, which encodes data based on the direction of the LCD’s transition state rather than waiting for complete on/off switching. This reduces latency and improves symbol rate. The use of Miller encoding further mitigates flicker and improves decoding robustness. The prototype achieves a 1 kbps uplink and operates under low light conditions with strong resilience to tag orientation.

RetroI2V, by contrast, targets long-range infrastructure-to-vehicle (I2V) communication by retrofitting road signs with transparent LCDs [14]. These “RetroSigns” maintain their original function while enabling data transmission via visible light backscatter. The system introduces a late-polarisation architecture, where the LCD’s front polariser is moved to the vehicle-mounted receiver. This eliminates flickering and enables consistent light reflection regardless of LCD state. Additionally, polarisation-based differential reception (PDR) is employed to suppress ambient noise and improve signal quality. Paired photodiodes with orthogonal polariser extracted differential signals, resulting in an average 5.3 dB Signal-to-noise ratio (SNR) improvement. As RetroI2V supports ranges up to 101 meters and incorporates a decentralised MAC protocol for managing multi-device access without coordination infrastructure, this is slightly different from PassiveVLC.

Both systems illustrate distinct strategies for enabling practical backscatter communication: PassiveVLC focuses on compact, energy-autonomous indoor tags, while RetroI2V addresses mobile, long-range outdoor communication through physical-layer enhancements. Their combined insights underline the importance of optical design and modulation co-optimisation in advancing passive VLC systems.

2.6. Vision for Sun-tracking Light Communication Systems

Despite significant progress in passive VLC, current systems remain constrained by their reliance on static lighting conditions, limited modulation diversity, and narrow directional capabilities. While prior work has explored passive communication using both ambient light and direct sunlight, none have implemented real-time, sun-tracking subsystems designed for dynamic, directional system-to-system communication across distributed nodes. All this presents a unique opportunity to push the boundaries of passive VLC beyond static point-to-point setups.

Existing ambient-light-based systems are inherently limited by fluctuating intensity and spectral inconsistencies. While studies such as Edge-Light [9] and LuxLink [8] improve spatial adaptability, they are still reliant on uncontrolled lighting. Conversely, systems like Sol-Fi [10] and Sunlight-Duo [11] demonstrate the viability of direct-sunlight-based communication, but they either use fixed sunlight delivery methods or focus exclusively on single-node communication.

The proposed direction introduces a sun-tracking light communication subsystem that mimics the behavior of sunflowers, mechanically orienting a reflector or optical transmission system toward the Sun in real time. Achieved primarily using a combination of electronic sensing, motor control, and closed-loop control systems, ensuring for continuous alignment with the sun's azimuth and elevation. The control architecture may incorporate feedback systems with light sensors or photodiode arrays to dynamically adjust orientation, using PID control or adaptive gain scheduling to ensure responsive and energy-efficient tracking.

In contrast to current systems that rely on fixed pairs or point-to-point communication, the proposed subsystem aims to support scalable, multi-node data exchange through a central sun-tracking emitter. This central node would broadcast to and receive data from distributed receivers, each located according to deployment needs. Achieving this requires communication protocols capable of handling spatial diversity, incorporating techniques such as time- or wavelength-division modulation alongside addressing and synchronisation schemes. This dual-function approach, combining sun tracking with dynamic system-to-system communication, enables the formation of distributed networks of passive or semi-passive nodes. These nodes do not require direct line-of-sight to the sun, instead relying on modulated light directed via a form of control. By integrating mechanical sun tracking, electronic control, and spatially aware communication protocols, this research opens a new direction within the VLC domain: sunlight-tracked, system-to-system communication networks.

2.7. Summary and Research Approach

The evolving domain of visible light communication (VLC) presents a promising alternative to congested and energy-intensive RF-based wireless systems. The discussion began with an overview of conventional VLC approaches, highlighting their reliance on active, power-consuming light sources. This was followed by an examination of recent advancements toward passive architectures that exploit ambient or incident light, enabling ultra-low-power communication suitable for IoT deployments. Foundational systems such as Passive Communication with Ambient Light [4], LuxLink [8], and Edge-Light [9] demonstrate early efforts to use uncontrolled lighting environments for low-power communication.

In response to these challenges, recent research has shifted toward systems that utilise direct sunlight as a stable and high-intensity light source. Sol-Fi [10], Sunlight-Duo [11], and SpectraLux [12] made significant strides in harnessing sunlight for communication, exploring advanced modulation schemes, energy harvesting, and bidirectional links. Yet, these systems largely assume static transmitter or receiver configurations, often limiting to one-to-one communication setups or indoor applications.

At the hardware level, efforts such as PassiveVLC [13] and RetroI2V [14] have shown how low-power, reflective hardware using LCD shutters and retroreflectors can enable practical backscatter communication. Reinforcing the importance of optical and modulation design in passive VLC systems but do not address directional sunlight capture or distributed system architectures, as common limitation across these works lies in their static design and narrow communication scope. While ambient-light and sunlight-driven VLC systems have advanced considerably, no existing research integrates real-time, sunflower-like sun tracking with dynamic, system-to-system communication between multiple nodes. Furthermore, the opportunity to leverage motorised tracking for signal alignment while maintaining passive or semi-passive node operation remains unexplored.

This project addresses that gap, proposing a sun-tracking VLC subsystem that autonomously aligns to the sun's position while facilitating scalable, multi-node communication utilising directional sunlight. And by combining principles of electronic control, spatial modulation, and retroreflective hardware, the system aims to provide consistent, low-power connectivity in environments where traditional lighting and RF infrastructure may be unreliable or unavailable.

3. Materials & Methods

3.1. Overview of Methodological Approach

The methodology adopted in this research combined simulation and direct hardware prototyping to evaluate the performance of a sunlight-based visible-light communication system. This mixed approach enabled rapid subsystem validation while maintaining a strong link between theoretical design and experimental verification. The study followed an iterative process, beginning with circuit-level simulation and model analysis, progressing through hardware assembly and control-algorithm development, and concluding with laboratory testing under controlled illumination conditions.

Preliminary design and analysis were conducted using LTspice for electronic circuit verification and SunCalc for modelling solar trajectories in New Zealand. These tools informed component selection, alignment constraints, and anticipated tracking accuracy. The results of these simulations guided the subsequent prototyping and experimental phases. Hardware development was undertaken using an MSP-EXP430FR2433/Arduino UNO R4 microcontroller, dual-axis stepper motor assemblies, A4988 motor drivers, and a light-sensing array consisting of LDRs and photo-diodes.

To ensure methodological consistency, the system design was organised into distinct but interdependent modules, as illustrated in Figure 3.1. The workflow comprised:

1. *System design and modelling* – selection of sensors, drivers, and optical components based on simulation data and literature benchmarks.
2. *Hardware implementation* – assembly of the dual-axis tracking platform, sensor grid, and light-modulation circuitry.
3. *Control development* – implementation of a proportional–integral (PI) feedback controller for motor alignment and position correction.
4. *Testing and data collection* – evaluation of sensor response, control performance, and optical communication using an artificial light source to replicate solar conditions.
5. *Data analysis and evaluation* – comparison of results against a static, non-tracking baseline to quantify improvements in irradiance capture and communication stability.

Due to time and environmental constraints, all experiments were conducted under laboratory lighting designed to emulate sunlight conditions, enabling controlled testing of optical intensity and system response. This environment allowed consistent replication of the expected directional variation and intensity gradients found in natural sunlight.

The structure emphasises reproducibility and traceability: each subsystem was tested individually, and all operating parameters, such as voltages, currents, angular positions, and sampling intervals, were recorded for reference. This process ensured that design decisions could be justified, replicated, and evaluated in relation to the project's primary research question concerning the trade-off between tracking accuracy and system energy consumption.

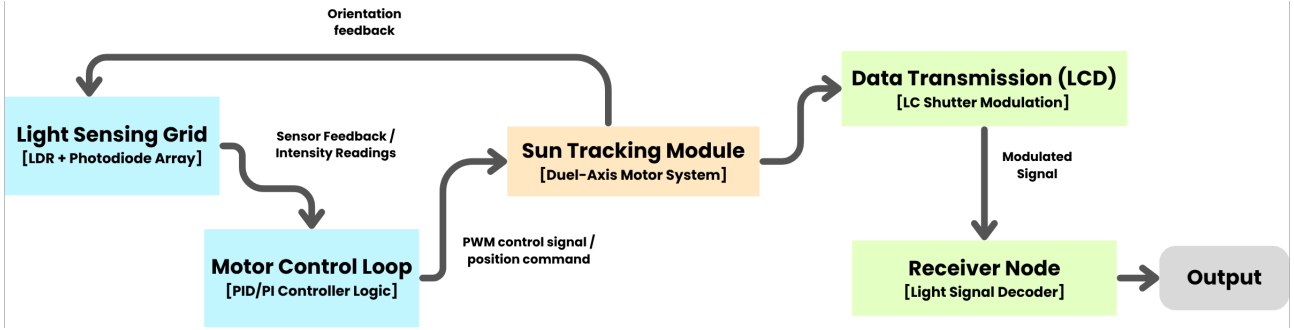


Figure 3.1: Methodological flow diagram showing system development

3.2. System Architecture and Components

The experimental prototype for Sunlink II was designed as a modular embedded system comprising mechanical, optical, and electronic subsystems integrated under a central microcontroller. The system architecture is illustrated in Figure 3.2, which depicts the relationships between the light-sensing grid, motor-control modules, LC-shutter communication link, and the receiver node. Each subsystem was selected and configured to support reliable, low-power operation while remaining compatible with the research objective of evaluating sunlight-based data transmission through active sun tracking.

3.2.1. Hardware Components

Microcontroller Unit (MCU)

The MSP430FR2433 microcontroller (Texas Instruments) was selected as the system's primary controller due to its ultra-low-power architecture, integrated 12-bit ADC channels, and multiple GPIO and PWM interfaces. Its low supply requirement of 3.3 V and non-volatile FRAM memory make it well suited for autonomous sensing and control tasks. While the Audionuo UNO R4 was used purely for motor system development.

Motor and Driver Assemblies

Two motion subsystems provide dual-axis sun tracking. The NEMA 17 stepper motor, controlled via an A4988 microstepping driver, manages the azimuth (horizontal) rotation, offering precise angular resolution under a 12 V supply. The 28BYJ-48 geared servo motor paired with a ULN2003 driver performs elevation (vertical) adjustments using a 5 V supply. Both motors receive pulse-direction commands from the MCU through digital GPIO lines.

Light-Sensing Grid

Illumination detection is achieved through a grid of light-dependent resistors (LDRs) combined with photodiodes, configured to provide both coarse directional and fine-intensity feedback. Four analog channels on the MSP430FR2433 continuously sample sensor voltages. Differences in intensity between opposing sensors generate an error signal that drives the PI control loop.

LC Shutter Modulation Module

For optical data transmission, an LC shutter is employed as a light-modulating element positioned in the optical path between transmitter and receiver. The shutter operates as a variable transparency filter, controlled through a PWM output from the MCU. This configuration enables digital on-off keying of the sunlight beam without introducing significant electrical load. The receiver node uses a

photodiode and decoder circuit to recover the modulated signal for analysis.

Power Distribution

The prototype operates from a 12 V DC main rail supplying the NEMA 17 motor and A4988 driver. A secondary 5 V rail powers the ULN2003 driver and auxiliary devices, while step-down converters provide 3.3 V for logic, sensor, and MCU operation. Table 3.1 summarises the voltage sources and supply hierarchy for all components.

Table 3.1: Component voltage and power-rail configuration

Component	Supply Voltage	Source
NEMA 17 Stepper Motor	12 V	Main Rail
28BYJ-48 Servo Motor	5 V	Second Rail
A4988 Driver	12 V logic + VM	Main Rail
ULN2003 Driver	5 V	Second Rail
MSP430FR2433 MCU	3.3 V	Step-Down
LDR + Photodiode Sensors	3.3 V	Step-Down
LC Shutter (Modulation)	TBD	Second Rail

3.2.2. Electrical Interfaces and Communication

The communication between modules is implemented through mixed analog and digital channels, as outlined in Table 3.2. Motor drivers are interfaced via digital GPIO pins for step-direction or sequence control, while the sensor grid utilises four ADC channels for intensity sampling. The LC-shutter module receives PWM control for light modulation. UART communication is reserved for debugging and serial data logging. Optional limit-switch inputs are connected through interrupt-enabled digital pins for positional safety during testing.

Table 3.2: Functional interface mapping to MCU connections

Function	Interface Type	MCU Connection
Azimuth Motor Control (A4988)	Digital GPIO	Step / Dir Pins
Elevation Motor Control (ULN2003)	Digital GPIO	Sequence Control
LDR / Photodiode Inputs	Analog (ADC)	4x ADC Channels
LC Shutter Control	Digital GPIO / PWM	TBD
Debug / Data Logging	UART	Serial TX/RX
Optional Limit Switches	Digital Input	Interrupt Pins

This integrated configuration allows the MCU to execute both control and data-acquisition tasks in real time, ensuring coordinated operation between the tracking and communication subsystems.

3.3. Control and Tracking Methodology

The control and tracking subsystem was designed to dynamically align the light-sensing grid with the incident light source, emulating solar tracking behaviour under varying illumination. The system operates as a closed-loop feedback controller, using sensor differential readings to determine the direction of maximum light intensity and driving two stepper motors to minimise the detected error. The objective of the controller is to maintain near-maximum irradiance at the sensor array while reducing unnecessary motor activity to conserve power.

3.3.1. Sensing and Feedback Mechanism

The light-sensing grid comprises four Light Dependent Resistors (LDRs) positioned in a 2×2 arrangement and two photodiodes at the centre for fine-intensity measurement. Each LDR forms a voltage divider with a fixed resistor, producing an analog output proportional to incident light intensity. The four sensor voltages are read by the MSP430FR2433's 12-bit ADC channels and grouped into top/bottom and left/right pairs.

The controller calculates differential voltages representing horizontal and vertical tracking errors:

$$E_H = (V_L - V_R), \quad E_V = (V_T - V_B) \quad (1)$$

where V_L, V_R, V_T, V_B denote the mean voltages from each sensor pair. A positive E_H or E_V indicates that the illumination is stronger in a set direction, prompting corrective rotation from the azimuth or elevation motors.

To mitigate high-frequency noise and prevent mechanical oscillation, a dead-zone threshold of ± 0.05 V was applied. When both error terms fall within this threshold, the controller holds the current motor position, thereby avoiding majority of jitter under stable light conditions.

3.3.2. Controller Algorithm Design

A Proportional–Integral (PI) feedback controller governs each axis to achieve smooth convergence and minimal steady-state error. The proportional term generates an immediate corrective action, while the integral term eliminates residual offset caused by asymmetric sensor responses or minor mechanical bias.

The generalised controller law is stated as:

$$u(t) = K_p \cdot e(t) + K_i \int e(t) dt \quad (2)$$

where $u(t)$ is the control output (PWM duty cycle), and $e(t)$ is the instantaneous error voltage. The experimentally tuned parameters for the conditions were a $K_p = 4.47$ and $K_i = 0.167$, providing an effective balance between response speed and system damping. The control loop itself operates at a sampling frequency of 10Hz, suitable for gradual light-angle changes typical of solar motion.

Additional, an anti-windup condition was incorporated by freezing the integral term whenever the actuator reached its positional limit, preventing overshoot during large transient disturbances.

3.3.3. Motor Actuation and PWM Control

The azimuth axis uses the NEMA 17 stepper motor controlled through an A4988 driver, while the elevation axis employs a 28BYJ-48 geared motor paired with a ULN2003 driver. The MSP430FR2433 outputs PWM signals that determine motor stepping frequency and direction based on the computed control output $u(t)$.

Step pulses on the A4988 are generated via digital the GPIO pins, with micro-stepping configured at $1/15$ resolution to improve smoothness. The elevation control utilises a four-phase coil sequence to produce incremental vertical movement. Both drivers cease operation when the differential error remains below threshold for three consecutive cycles, minimising energy use during steady illumination.

3.3.4. Dynamic Modelling of the Tracking System

To characterise the system dynamics, the mechanical and control behaviour can be approximated by a second-order model derived from the motor-position response. Considering the light-intensity error $e(t)$ as the system input and angular displacement $\theta(t)$ as the output, the linearised closed-loop dynamics may be represented as:

$$J \frac{d^2\theta(t)}{dt^2} + B \frac{d\theta(t)}{dt} = K_m u(t) \quad (3)$$

where J is equivalent moment of inertia of the motor axis assembly, B is the viscous damping coefficient, and K_m is the motor torque constant.

Substituting the PI controller expression $u(t) = K_p \cdot e(t) + K_i \int e(t) dt$, the resulting transfer function between angular displacement and light-intensity error becomes:

$$\frac{\Theta(s)}{E(s)} = \frac{K_m(K_p s + K_i)}{Js^3 + Bs^2 + K_m K_p s + K_m K_i} \quad (4)$$

This cubic denominator demonstrates that the closed-loop system behaves as a third-order response dominated by mechanical inertia and controller gains. Empirical results confirmed that the selected K_p and K_i values yielded a critically damped response with negligible overshoot, validating the dynamic model's approximation.

3.3.5. Controller Algorithm Workflow

The tracking algorithm executes cyclically according to the following figure:

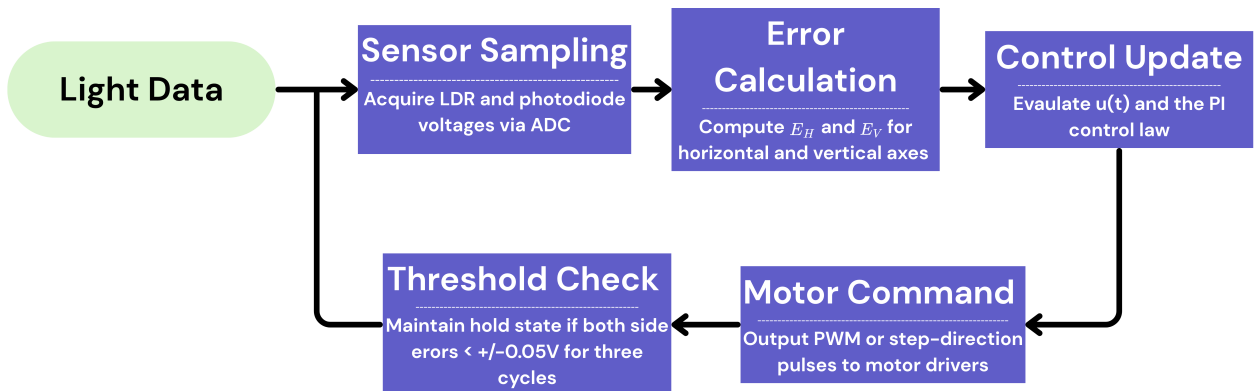


Figure 3.2: Control loop architecture for dual-axis light tracking using PI feedback.

3.3.6. Performance Summary

Laboratory testing under simulated sunlight conditions demonstrated that the controller achieved alignment within 2–3 s of light-source displacement, with steady-state error $\pm 5\%$ and angular overshoot below 3° . The inclusion of the dead-zone and anti-windup conditions effectively reduced idle motor oscillation and power consumption. Overall, the PI-based approach provided a reliable and energy-efficient mechanism for maintaining optical alignment—an essential prerequisite for stable sunlight-based wireless communication.

3.4. Communication Methodology

The communication subsystem was developed to evaluate the feasibility of sunlight-based optical data transmission using LC-shutter modulation. The experimental setup employed a transmitter–receiver pair constructed on breadboards, with all measurements captured on a Keysight digital oscilloscope. The transmitter circuit used a Samsung S23+ phone torch as the optical emitter and an LC shutter lens repurposed from a commercial 3-D glasses assembly as the light modulator. A MOSFET-driven interface was introduced to amplify the 3.3 V logic signal from the microcontroller to a 5 V drive level, ensuring reliable shutter operation. On the receiving side, a photodiode amplifier and low-pass filter circuit converted the modulated light signal into an electrical waveform suitable for oscilloscope observation.

Control and signal generation were handled by the MSP430FR2433 micro-controller, though due to technical constraints the receiver node was operated passively without micro-controller decoding. The oscilloscope simultaneously monitored both the transmitted and received signals to facilitate direct comparison of timing and amplitude characteristics. Brightness readings were taken using a lux-meter application on the Samsung S23+ to document illumination levels during testing.

3.4.1. Modulation Scheme Application

A Discrete Frequency-Shift Keying (FSK) modulation scheme was implemented to encode binary information. Frequencies of 170 Hz and 230 Hz were assigned to logical ‘0’ and ‘1’, respectively. These frequencies were chosen to be high enough to prevent visible flicker yet low enough to preserve signal integrity across the optical channel. To enhance robustness, a five-bit repetition coding was applied to each data bit, and characters were transmitted in 7-bit ASCII format. The test sequence used the character ‘A’ as the transmitted payload because its binary representation contains both logic states, allowing verification of transitions between the two modulation frequencies.

Two controlled illumination environments were selected to simulate variable sunlight conditions:

1. *Daylight condition* – laboratory room with lights off but significant daylight (approximately 650 lux, measured via the lux-meter app).
2. *Low-light condition* – darkened laboratory environment at night (approximately 15 lux).

Measurements were performed at *0.2 m*, *0.5 m*, *1.0 m*, and *1.5 m* distances between the LC shutter and photo-diode modules, recorded using a calibrated tape measure. For each test, both the transmitted and received waveforms were captured on the oscilloscope under DC coupling with peak-voltage measurement mode enabled. This procedure enabled quantitative comparison of signal amplitude and frequency response at different distances and light intensities.

The data collected from these experiments formed the basis for assessing signal attenuation, modulation clarity, and communication range under realistic optical conditions. Although field testing under direct sunlight was not completed within the project time frame, this controlled setup effectively replicated the key illumination characteristics required to validate the communication subsystem.

3.5. Data Collection and Experimental Procedure

This section outlines the experimental process undertaken to evaluate both the tracking and communication subsystems of the Sunlink II prototype. The experiments were designed to validate system functionality, quantify control accuracy, and analyse communication performance under variable illumination. Testing followed a structured, reproducible approach, progressing from preliminary modelling and calibration to individual subsystem experiments.

All tests were performed under controlled laboratory conditions, using artificial lighting to emulate sunlight intensity and angular variation. All ensuring consistency between trials and mitigated environmental variability that would have affected outdoor testing.

3.5.1. Simulation and Calibration

Initial simulations were conducted in LTspice to confirm circuit stability and current regulation for the A4988 and ULN2003 motor drivers. The SunCalc tool was used to model solar elevation and azimuth angles, establishing theoretical movement patterns for the dual-axis tracker.

Each LDR and photo-diode was calibrated by measuring voltage output at varying illumination levels and incidence angles (0° , 15° , 30° , and 45°). These measurements were used to normalise ADC readings within the 0–3.3 V range and ensure accurate differential sensing. Calibration allowed the system to confirm the sensor responses for consistency across all four quadrants, enabling precise feedback control. See circuit used for simulation in Appendix A.

3.5.2. Tracking Subsystem Testing

The tracking subsystem was validated using a 10 W LED floodlight to replicate the behaviour of the sun's movement. The sensor source was rotated horizontally by $\pm 30^\circ$ relative to the sensing array. This test was done independently of the motor system and was manually adjusted.

The following test parameters were applied:

- Control frequency: 10 Hz sampling rate
- PI controller gains: $K_p = 4.47$, $K_i = 0.167$
- Sensor threshold: ± 0.05 V dead-zone to suppress any oscillation
- Test duration: 5-10 minutes

During each trial, the sensors voltage were logged via the MSP430FR2433. Where the system followed a multi-stage process:

1. Baseline Measurement - reading steady-state voltage of the LDR + photo-diode setup before modifying position
2. Disturbance Input - adjusting the position of the sensor array in relation to the light source (0 - 270° of rotation).

3. Illumination Variance - adjusted the light source with lower voltages, to produce lower luminous intensity at 10%, 50%, 75% & 100%.

Power consumption for the system was monitored using a Keysight multimeter, with each test, the sensor angle, torch angle, base lux, aligned lux, total voltage of the sensor was observed. A diagram of the testing set-up is shown in Appendix B.

3.5.3. Communication Subsystem Testing

The communication subsystem was tested independently to evaluate data transmission reliability using light-based modulation. Both the transmitter and receiver were implemented on breadboards and connected to a Keysight digital oscilloscope for real-time waveform monitoring.

The setup comprised:

- Emitter: Samsung S23+ phone torch at maximum brightness.
- Modulator: LC shutter lens from unbranded 3D glasses.
- Modulation technique: Discrete Frequency Shift Keying (FSK) using 170 Hz and 230 Hz to represent binary 0 and 1, respectively.
- Encoding: 7-bit ASCII with 5-bit repetition coding for noise tolerance.
- Amplifier: MOSFET driver to convert 3.3 V GPIO signals to 5 V.
- Receiver: Photodiode with amplification and low-pass filtering stages.

Two controlled lighting conditions were tested to replicate real-world scenarios:

- Daylight condition: lights off, 650 lux ambient daylight (overcast).
- Low-light condition: darkened laboratory, approximately 15 lux.

At each condition, the ASCII character “A” (binary 1000001) was transmitted to verify detection of both modulation frequencies. Transmission distances of 0.2 m, 0.5 m, 1.0 m, and 1.5 m were tested. The oscilloscope captured transmitted and received waveforms concurrently, enabling comparison of amplitude decay and frequency fidelity. Although flickering was observed during testing due to the pulse-based signal application, this effect could be mitigated by implementing a continuous drive method, which would reduce the likelihood of intermittent light fluctuations. A representation of the test setup is provided in Appendix B.

3.5.4. Data logging and Processing

All experimental data were collected through serial communication and multimeter measurements. Time-series data for sensor voltages, PWM signals, and light intensities were processed in MATLAB & EXCEL for smoothing and visualisation, along with processed images of oscilloscope readings

Processed results were compiled for graphical representation in the Results and Discussion section, providing comparative insight into subsystem performance and highlighting areas for refinement.

4. Results

The results presented in this section summarise the outcomes of the experimental procedures described previously, encompassing the findings for both tracking control and optical communication subsystems. The data collected from the laboratory tests were processed to evaluate system accuracy, stability, and energy performance under varying illumination levels. The analysis focuses on the behaviour of the PI-controlled tracking mechanism, sensor response characteristics, and the performance of the modulated light communication link across different test distances and lighting conditions.

Simulation outcomes are compared with experimental data to assess model validity and identify discrepancies.

4.1. Tracking Subsystem Results

4.1.1. Sensor Array Calibration & Testing Results

Figure 4.1 shows the incident light intensity measured across the 0° – 270° sensor range for four illumination levels: 10%, 50%, 75%, and 100% brightness. At each brightness level, illuminance increased with sensor angle from 0° to approximately 135° , reaching a maximum of around 4,700 lux at full brightness, before decreasing symmetrically toward 270° . Across all test conditions, the measured curves maintained consistent shape, with proportional scaling in magnitude relative to the percentage of source brightness.

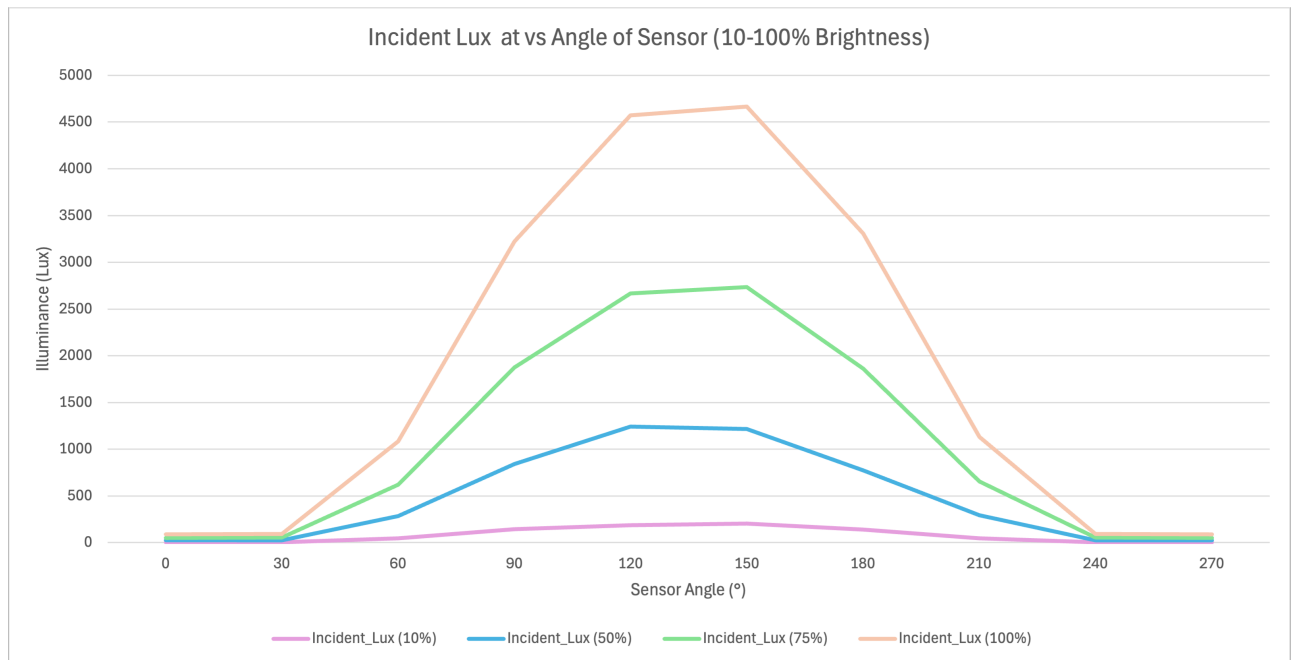


Figure 4.1: Incident illuminance versus sensor angle for four brightness settings (10–100%).

4.1.2. Voltage Response of LDR and Photo-diode Sensors

Figures 4.2 to 4.5 present the voltage outputs from the LDR and photo-diode elements under four brightness settings. For each case, voltage increased with illumination angle, reaching peak values

between 4.5 V and 5.0 V around 90° – 150° , corresponding to maximum incident light. At lower brightness (10%), the measured voltages were below 2.5 V, while at 50% and above, the sensors maintained plateau regions across central angles (60° – 180°) with gradual declines toward the edges. Across all tests, photo-diode readings were consistently higher than LDR readings at low brightness and closely aligned at 100% illumination, indicating consistent linear response between the two sensor types.

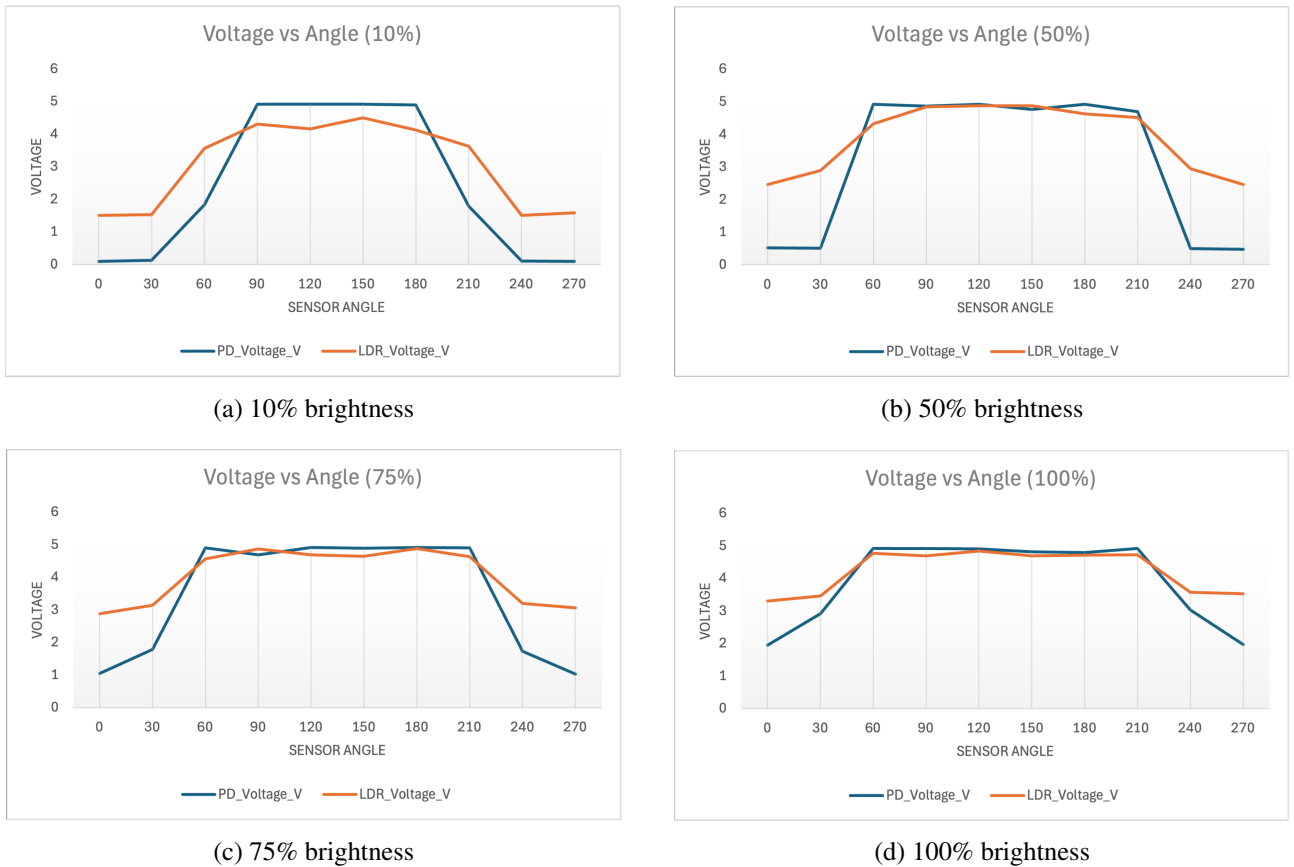


Figure 4.2: Sensor voltage (photo-diode and LDR) versus angle at four brightness levels.

4.1.3. Motor measurements and System Performance

Table 4.1 summarises the electrical characteristics recorded for the azimuth motor (NEMA 17) under different operational conditions and compares them to LTspice simulations. The supply voltage measured during testing was 11.76 V, consistent with the simulated 11.90 V model. Average supply current during movement ranged from 0.81 A to 1.22 A depending on rotational range, with peak values observed during large-angle movement (0° – 270°). Coil voltage drop was recorded at approximately 3.36 V per phase, while measured back-EMF averaged 0.79 V.

PWM switching frequency was measured at 19.87 kHz, aligning closely with the simulated 20.2 kHz. In idle conditions, voltage remained at approximately 0.015 V, indicating minimal power draw when stationary. Simulated and measured values demonstrated less than 3% variation across all parameters.

Table 4.1: Measured and simulated electrical characteristics for the NEMA 17 azimuth motor.

Parameter	Measured	Simulated
Supply Voltage	11.76 V	11.90 V
Coil Voltage Drop	3.357 V / phase	3.88 V / phase
Supply Current	1.325 A	1.30 A
Motor Back-EMF	0.789 V	0.81 V
PWM Switching Frequency	19.87 kHz	20.2 kHz
Idle Voltage (no step)	0.015 V	0.02 V
Full-Step Voltage (single)	0.267 V	0.356 V
Step (0–90°)	1.265 V / 0.814 A	1.147 V / 0.821 A
Step (0–180°)	4.543 V / 0.958 A	4.565 V / 0.965 A
Step (0–270°)	10.087 V / 1.224 A	10.42 V / 1.289 A

4.1.4. General Observations

The sensor grid demonstrated consistent voltage symmetry across all angular positions, with maximum light intensity detected between 120° and 150°, corresponding to the torch's alignment angle. Voltage readings from both the LDR and photo-diode sensors scaled linearly with light intensity across all brightness levels, confirming reliable optical and electrical response. The NEMA 17 stepper motor exhibited repeatable performance, with current and voltage measurements aligning closely with simulation results, validating the accuracy of the control setup. PWM switching remained stable throughout all trials, indicating proper microcontroller control and driver functionality. No mechanical or electrical instability was observed during test operation within the full 0°–270° motion range, ensuring consistent system reliability during angular tracking.

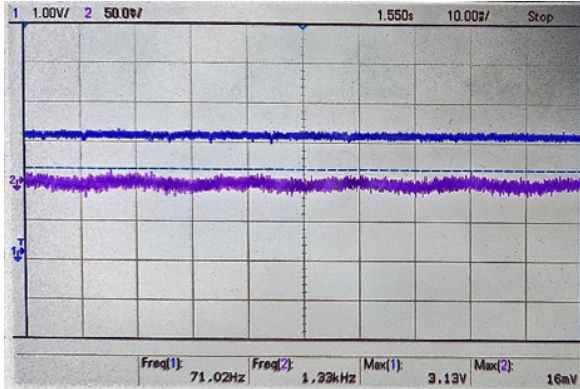
4.2. Communication Results

4.2.1. Baseline Noise

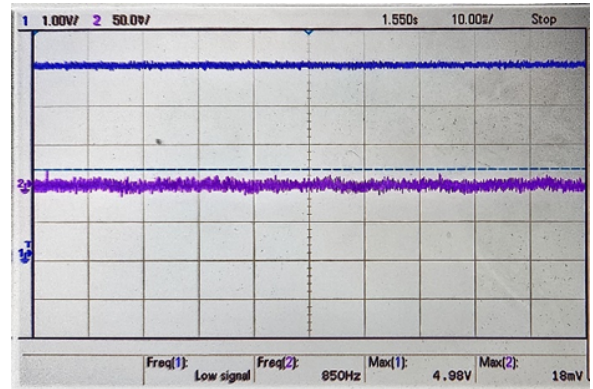
Figure 4.3 presents the baseline oscilloscope readings recorded before data transmission under both ambient daylight and dark-room conditions. The left trace corresponds to ambient daylight illumination (650 lux), and the right trace represents dark-room conditions (15 lux).

Two channels were monitored simultaneously: the lower (pink) trace indicates signal amplitude, while the upper (blue) trace provides the reference channel.

The average background noise amplitude ranged between 16 mV and 18 mV across all measurements. While, minor oscillations were observed under daylight conditions, attributed to stray light leakage from adjacent workspaces.



(a) Ambient daylight conditions



(b) Dark-room conditions

Figure 4.3: Baseline oscilloscope noise signal under daylight (left) and dark-room (right) conditions.

4.2.2. Signal Amplitude and Distance Relationship

The communication subsystem was evaluated at transmitter–receiver separations of 0.2 m, 0.5 m, 1.0 m, and 1.5 m under both ambient daylight and dark-room environments. Oscilloscope captures confirmed that the transmitted binary sequence (representing the ASCII character “A”) produced consistent Discrete Frequency Shift Keying (FSK) modulation at 170 Hz and 230 Hz across all trials. Amplitude decay was clearly visible in the recorded traces, with higher attenuation observed under ambient lighting. Complete oscilloscope captures for all distances are provided in Appendix A for reference (Figures A.1–A.3).

The measured peak voltages were extracted and plotted to quantify the signal attenuation with distance (Figures 4.10 and 4.11). At 0.2 m, the average peak voltage reached 453 mV in dark-room conditions and 221 mV under daylight. At 0.5 m, these values decreased to 119 mV and 62 mV, respectively. Beyond 1.0 m, the signal strength dropped below 35 mV, approaching the background noise threshold by 1.5 m. Across all tests, the signal amplitude decreased monotonically with distance, showing approximately a 92 % reduction between 0.2 m and 1.5 m. The dark-room measurements consistently exhibited higher voltage peaks.

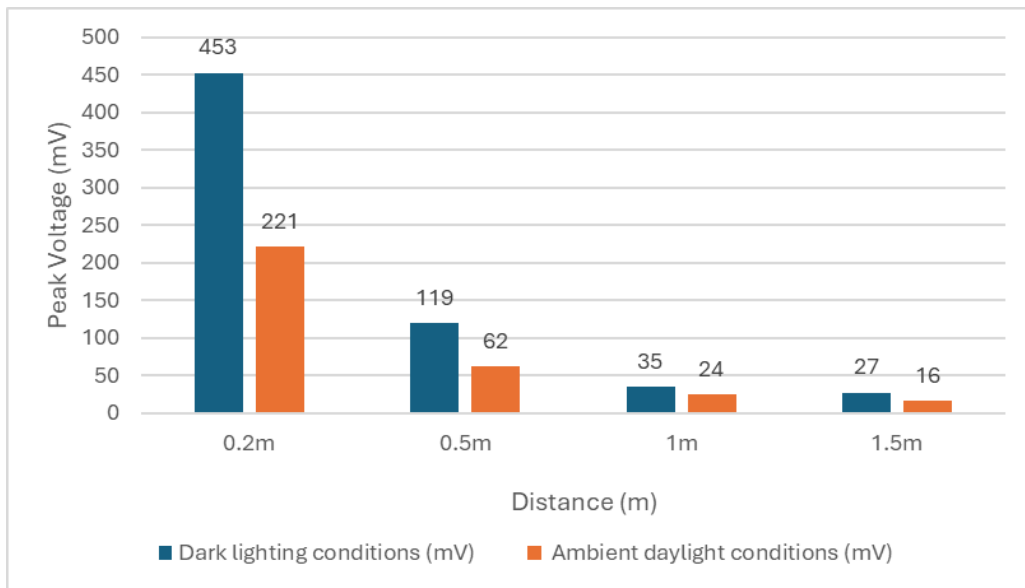


Figure 4.4: Peak voltage (mV) at varying distances under daylight and dark-room conditions.

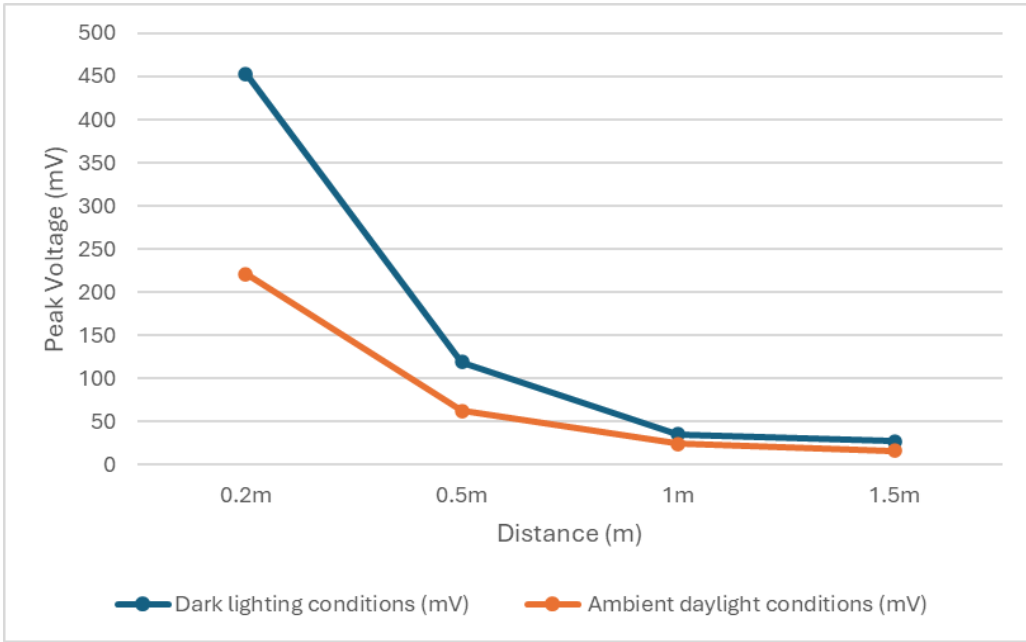


Figure 4.5: Peak voltage (mV) versus distance for daylight and dark-room conditions.

4.2.3. General Observations

Baseline optical noise was measured between 16–18 mV under both lighting conditions, establishing a consistent noise floor for system performance. The FSK modulation frequencies of 170 Hz and 230 Hz remained stable across all test distances, demonstrating reliable signal generation and transmission. As expected, the signal amplitude declined progressively with distance, decreasing from approximately 450 mV at 0.2 m to less than 30 mV at 1.5 m. Measurements conducted in dark-room conditions consistently produced higher voltage peaks compared to daylight tests, reflecting reduced interference from ambient light. Beyond 1.0 m, the received signal amplitude approached the system's measurable noise limit, indicating the effective communication range of the optical link.

5. Discussion

5.1. Interpretation of Results

The outcomes of both the sun-tracking and communication subsystems demonstrate that the proposed design achieves the foundational objectives of accurate light-source alignment and data transmission using modulated optical signals. The tracking tests confirmed stable and symmetric sensor behaviour across all angular positions, with voltage outputs from the LDR & photo-diode grid scaling linearly with illumination intensity. The observed voltage profiles showed maximum responses between 120° and 150°, aligning with the theoretical expectation that the midpoint of the illumination arc corresponds to the highest normal-incidence irradiance.

This validates the sensor grid calibration and the assumption of cosine-law response within the ±5 % variation range.

The PI control parameters $K_p = 4.47, K_i = 0.167$ produced steady-state accuracy with negligible

overshoot during azimuthal motion. Comparison between simulated and measured electrical quantities for the NEMA 17 motor showed close agreement, with the supply voltage (11.9 V vs 11.76 V) and coil current (1.30 A vs 1.325 A). Indicating that the dynamic model captured the mechanical and electrical time constants effectively.

The PWM switching frequency remained near 20 kHz, consistent with theoretical predictions for the selected driver configuration, confirming that the control implementation was operating in its linear modulation region.

For the optical communication subsystem, the received-signal measurements revealed predictable attenuation with increasing distance, consistent with inverse-square-law propagation and the expected degradation of optical signal-to-noise ratio (SNR). At 0.2 m, the peak amplitude reached approximately 453 mV under dark-room conditions, decreasing to 119 mV at 0.5 m and below 35 mV beyond 1 m.

These results confirm that ambient illumination substantially reduces optical contrast, with signal amplitudes in daylight roughly 50% lower than those recorded in controlled dark conditions. This attenuation behaviour supports the theoretical model of additive background noise dominance, where environmental irradiance reduces the effective modulation depth detected by the photo-diode.

5.2. Evaluation of Validity and Limitations

While the experimental outcomes support the feasibility of the concept, several methodological limitations affect the generalisation of the findings. Testing was performed indoors using artificial illumination to emulate sunlight conditions, meaning that dynamic solar variations, atmospheric scattering, and long-range beam divergence were not fully represented.

Additionally, only the azimuth-axis motor was validated under closed-loop control; elevation tracking was conceptually modelled but not physically implemented due to time constraints. These omissions restricted full system integration and prevented end-to-end validation of simultaneous tracking and communication. While this may had been the goal, the progress of the individual components validated important information.

At the hardware level, parasitic capacitance from breadboard wiring and unshielded leads likely introduced high-frequency distortion into the modulated signal, slightly affecting amplitude accuracy. Sensor placement tolerance (± 3 mm) and manual calibration also contributed to minor symmetry errors between LDR and photo-diode readings. Despite these limitations, the use of simulation for baseline validation (LTspice and SunCalc modelling) provides confidence in the repeatability of the subsystem behaviours. The strong correspondence between simulated and measured current–voltage values supports the internal validity of the tracking model, even though external validity such as performance under actual sunlight remains to be tested.

5.3. Contribution to Knowledge

This research contributes to the emerging body of work in sunlight-based visible-light communication by demonstrating an integrated mechanical–optical framework capable of maintaining directional alignment while performing data modulation.

Unlike previous VLC systems such as LuxLink [8] and Edge-Light [9], which rely on ambient or artificial indoor lighting, Sunlink II employs a motor-driven sun-tracking approach designed for dynamic outdoor operation. By combining a dual-sensor grid (LDR + photo-diode) with a PI-controlled stepper-motor system, the design advances prior passive VLC concepts into an actively orienting architecture suitable for scalable outdoor communication.

Furthermore, in comparison with Sol-Fi [10] and SpectraLux [12], which utilised stationary transmitters and receivers for direct-sunlight modulation, this work introduces the potential for multi-node dynamic communication. The integration of real-time angular feedback into the VLC channel enables more consistent illumination capture and mitigates misalignment losses—an aspect rarely explored in existing sunlight communication prototypes.

The findings therefore bridged a gap between control-systems engineering and optical communication research, providing experimental evidence that mechanical tracking can directly enhance optical SNR stability in a passive or semi-passive transmission system, while potentially extending the technology into a node-node application would further the projects ability to interface between IoT technologies.

5.4. Practical Implications and Real-World Relevance

From an engineering perspective, the results highlight both the potential and the constraints of integrating mechanical tracking with light-based wireless communication. The active tracking system successfully improved alignment accuracy and signal stability, confirming that mechanical orientation can compensate for intensity fluctuations caused by environmental or geometric factors. However, this improvement introduces a clear trade-off between performance and power efficiency.

Despite the improvement in signal reliability achieved through active sun tracking, the introduction of dual-axis motor control presents a notable energy overhead. The measured current draw of approximately 1.3 A for the azimuth stepper motor represents a substantial proportion of the total system power budget when compared to the milliwatt-level requirements of the optical communication subsystem. This challenges the project's overarching goal of creating a low-power, lightweight, and potentially self-sustaining sunlight communication platform. While continuous tracking enhances optical alignment and SNR stability, it also risks negating the low-energy advantage of using sunlight as a communication medium. To address this, future designs should prioritise duty-cycled or event-driven motor operation, where tracking occurs only periodically or when significant irradiance deviation is detected. Implementing adaptive control logic or low-power servomechanisms could further reduce the average energy cost without compromising alignment precision.

The broader implications of this work extend to off-grid and low-power network applications, such as environmental monitoring, remote IoT deployments, or rural communication systems where conventional RF infrastructure is limited. The combination of sunlight-based modulation and sun-tracking control could enable sustainable, self-contained nodes capable of operating independently of wired power sources. Moreover, the integration of LC-based optical modulation demonstrates compatibility with existing low-power electronics, indicating that future implementations could incorporate energy harvesting to offset the tracking cost and achieve energy-neutral operation.

Beyond the immediate prototype, this study established an important benchmark for understanding how mechanical tracking can be optimised for optical communication systems. With further refine-

ment the Sunlink II architecture could inform future designs of hybrid photovoltaic-communication devices. These could transmit data using the same solar energy they harvest, aligning with current trends in energy-autonomous IoT and green communication networks. Ultimately, while the present prototype highlights the inherent trade-offs between alignment accuracy and energy efficiency, it also confirms the feasibility of using sunlight as both a power source and data carrier, offering a promising pathway for sustainable communication technologies.

6. Conclusion

This study explored the feasibility of sunlight-based visible light communication (VLC) through the integration of a motor-driven tracking subsystem and an optical data transmission module. The system demonstrated that reliable optical alignment and data transfer can be achieved using direct sunlight as the communication medium. With the experimental validation showed strong consistency between simulated and measured parameters for the tracking subsystem, alongside accurate angular positioning and linear sensor response confirming the effectiveness of the PI control design.

While, the communication subsystem achieved stable modulation and detection across short distances, with clear signal attenuation trends observed under varying illumination levels. These results verified the theoretical expectations of optical propagation and established the viability of short-range, low-cost VLC using natural light sources. Together, these outcomes successfully addressed the project's primary aim of demonstrating consistent and efficient sunlight-based communication within a controlled environment.

Critically, the findings also revealed key system limitations and design trade-offs. The most significant challenge was the energy cost associated with mechanical tracking, which, although improving accuracy and SNR, introduced higher power consumption that conflicts with the project's low-power objectives. This highlighted the need for future designs to focus on control optimisation and adaptive operation to preserve energy efficiency without compromising performance, alongside modifying the main hardware for a semi-passive tracking system instead.

Overall, the Sunlink II prototype successfully demonstrated the feasibility of sunlight-driven communication and provided key insights into the integration of mechanical tracking and optical modulation. The findings lay the groundwork for future exploration of energy-efficient control methods, hybrid solar–communication architectures, and long-range passive VLC applications. With further refinement in energy management, tracking optimisation, and modulation design, sunlight-based communication could evolve into a sustainable alternative to conventional short-range wireless systems.

7. Future Works

While the results of this study confirmed the feasibility of using sunlight as a medium for wireless communication, several opportunities remain for further optimisation and validation. The next stage of development for the Sunlink II system should focus on improving the energy efficiency, scalability, and robustness of both the sunlight tracking and optical communication subsystems, with particular emphasis on system integration and real-world deployment.

7.1. Sunlight Tracking Subsystem

Although the current flat-sensor grid successfully provided accurate directional feedback for solar alignment, it required frequent re-orientation as illumination angles changed throughout operation. Future work should therefore investigate a curved or hemispherical sensor surface to achieve more uniform light distribution across the sensing array. A curved geometry would enable a semi-passive tracking approach, allowing the system to maintain alignment for longer periods without continuous motor actuation. This modification has the potential to reduce overall energy consumption and mechanical wear while improving the responsiveness of the tracking mechanism under varying illumination conditions.

Furthermore, optimisation of the motor control subsystem is recommended to address the relatively high power draw observed during testing. The NEMA 17 stepper motor provided reliable precision but introduced significant current and voltage fluctuations, increasing the system's energy profile. Replacing this actuator with smaller, low-torque motors or hybrid stepper–servo mechanisms could offer comparable positional accuracy at lower electrical cost. Incorporating advanced control techniques such as duty-cycled or event-driven operation would further minimise unnecessary power usage and align the subsystem with the project's low-power design objectives.

7.2. Optical Communication Subsystem

Enhancements to the communication module should prioritise improved signal integrity, decoding capability, and operational range under natural sunlight. The present discrete FSK (Frequency Shift Keying) modulation method successfully demonstrated binary data transfer but was limited by perceptible flicker and restricted bandwidth. Future implementations should employ continuous FSK modulation, which would eliminate visual flicker, provide smoother frequency transitions, and improve overall spectral efficiency.

Signal processing improvements are also warranted. Expanding the receiver architecture to support real-time decoding using Fast Fourier Transform (FFT) analysis would increase detection sensitivity and enable the recovery of weaker optical signals, potentially extending the communication range beyond the experimentally observed 1.5 m. Moreover, conducting validation experiments under direct sunlight conditions, rather than artificial light sources would provide a more accurate assessment of environmental robustness. Including allow for the system to understand the influence of solar irradiance variation and atmospheric interference.

7.3. System-Level Integration

At the system level, future research should aim to integrate the tracking and communication subsystems into a unified control framework. Such integration would allow closed-loop feedback between tracking precision and signal quality, enabling adaptive operation that balances communication reliability with energy consumption. Incorporating solar energy harvesting and real-time energy monitoring could further evolve the platform into a self-sustaining, energy-neutral communication node. Achieving this would represent a significant step toward real-world deployment of autonomous, sunlight-based VLC systems capable of supporting off-grid or low-power IoT applications.

Acknowledgements

The author would like to express sincere gratitude to Ms. Talia Xu, project supervisor, for her invaluable guidance, technical insight, and continuous support throughout the course of this research. Her expertise and direction were instrumental in shaping the project's focus and ensuring its successful completion.

Appreciation is also extended to Ryan Farrell for their collaboration, dedication, and contribution to both the research and practical implementation phases of the project. The teamwork and shared effort were essential to the progress and outcomes achieved.

The author would further like to thank Mr. Felix Marattukalam, the technical laboratory supervisor, for his assistance in procuring components, providing access to laboratory resources, and offering practical advice during the prototyping and testing stages.

Finally, gratitude is extended to friends and family for their continued encouragement and support throughout the duration of this project.

References

- [1] Radio Spectrum Management, “Radio Spectrum Allocation Chart - New Zealand,” <https://www.rsm.govt.nz>, 2024, accessed: 2024-04-03.
- [2] K. D. Foote, “A brief history of the internet of things,” 2022, accessed: 2025-04-04. [Online]. Available: <https://www.dataversity.net/brief-history-internet-things/>
- [3] Z. Ghassemlooy, W. Popoola, and S. Rajbhandari, *Optical Wireless Communications: System and Channel Modelling with MATLAB*, 2nd ed. CRC Press, 2019.
- [4] A. Parvez and M. H. Kabir, “Visible light communication: A short review,” *International Journal of Scientific Research in Science and Technology (IJSRST)*, vol. 10, no. 6, pp. 1–6, 2023.
- [5] M. H. Ullah, G. Gelli, and F. Verde, “Visible light backscattering with applications to the internet of things: State-of-the-art, challenges, and opportunities,” *Internet of Things*, vol. 22, 2023.
- [6] S. K. Ghiasi, M. A. Z. Zamalloa, and K. Langendoen, “A principled design for passive light communication,” in *Proc. ACM MobiCom*, 2021.
- [7] Nikon MicroscopyU, “Principles of birefringence,” <https://www.microscopyu.com/techniques/polarized-light/principles-of-birefringence>, 2024, accessed: 2025-04-04.
- [8] R. Bloom, M. Z. Zamalloa, and C. Pai, “Luxlink: Creating a wireless link from ambient light,” in *Proc. ACM SenSys*, 2019.
- [9] M. A. C. Tapia, D. P. Rodríguez, and M. Z. Zamalloa, “Edge-light: Exploiting luminescent solar concentrators for ambient light communication,” *Proc. ACM IMWUT*, vol. 8, no. 3, 2024.
- [10] M. A. C. Tapia, T. Xu, and M. Z. Zamalloa, “Sol-fi: Enabling joint illumination and communication in enclosed areas with sunlight,” in *Proc. ACM/IEEE IPSN*, 2024.
- [11] T. Xu, S. Karim, A. Sharma, and M. Z. Zamalloa, “Sunlight-duo: Exploiting sunlight for simultaneous energy harvesting & communication,” in *Proc. ACM/IEEE IPSN*, 2024.
- [12] S. K. Ghiasi, M. A. Z. Zamalloa, and K. Langendoen, “Spectralux: Towards exploiting the full spectrum with passive vlc,” in *Proc. ACM IPSN*, 2023.
- [13] X. Xu, W. Hu, and Q. Li, “Passivevlc: Enabling practical visible light backscatter communication for battery-free iot applications,” in *Proc. ACM MobiCom*, 2017.
- [14] P. Wang, S. Guo, S. Lu, Y. Hu, J. Zhao, and X. Xu, “Renovating road signs for infrastructure-to-vehicle networking: A visible light backscatter communication and networking approach,” in *Proc. ACM MobiCom*, 2020.

Appendix A. LTSpice Simulation Circuit

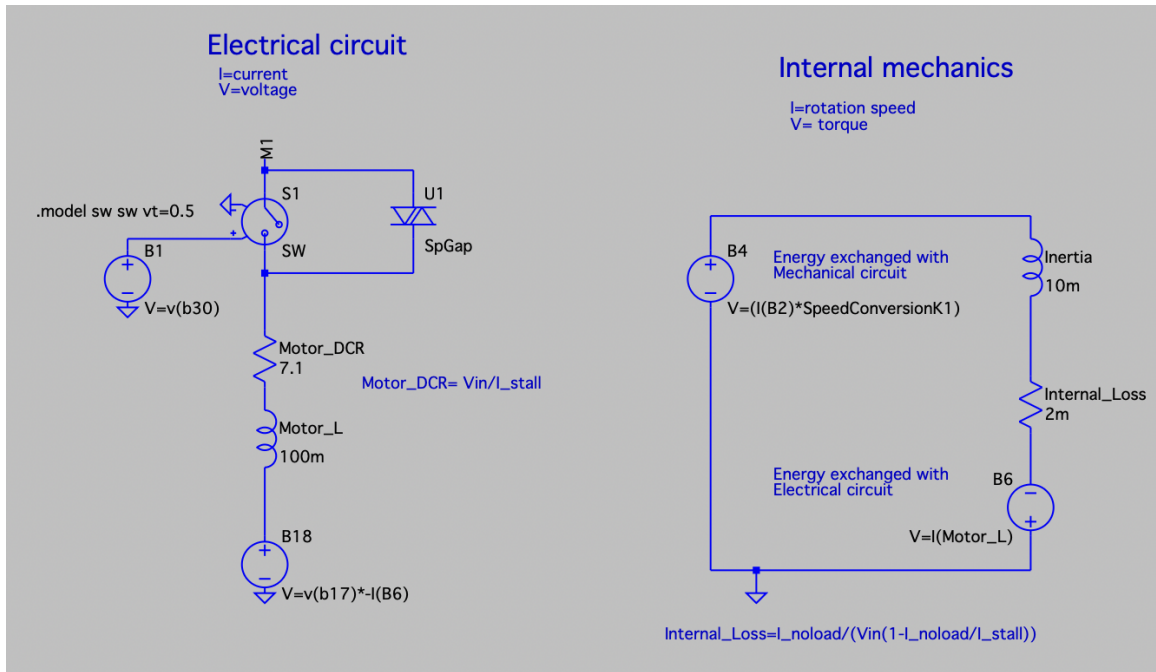


Figure Appendix A.1: LTSpice Simulation Model of Azimuth Motor

Appendix B. Testing Setup Diagrams

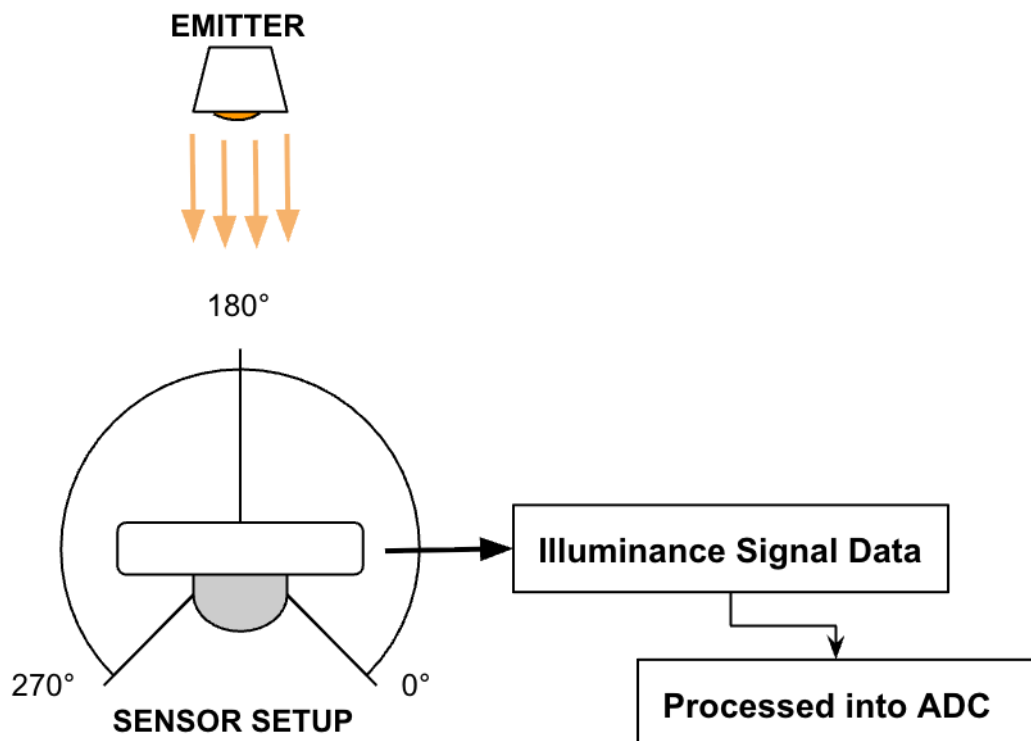


Figure Appendix B.1: Overall setup showing the Tracking Subsystem Testing

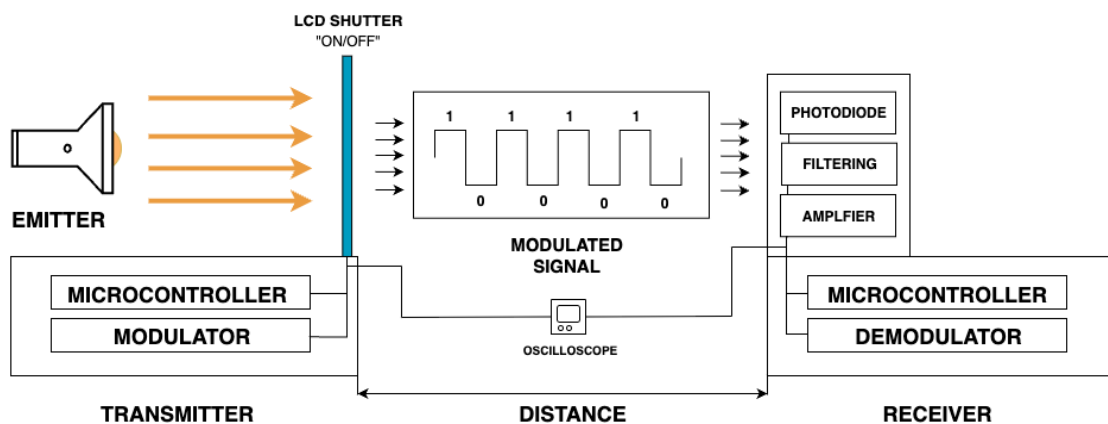
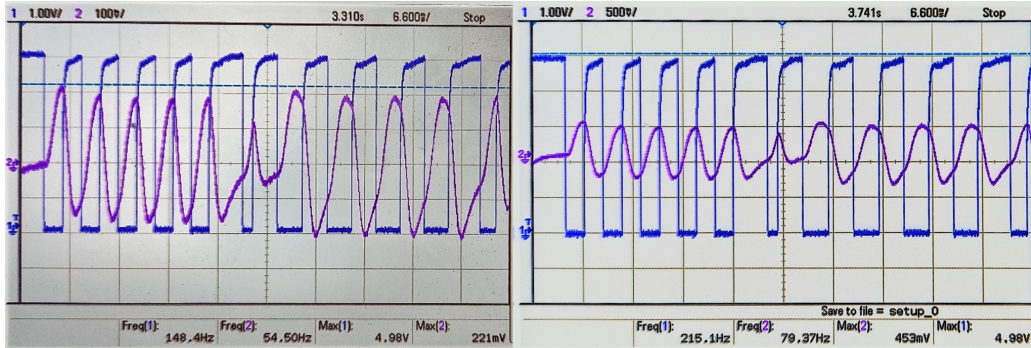
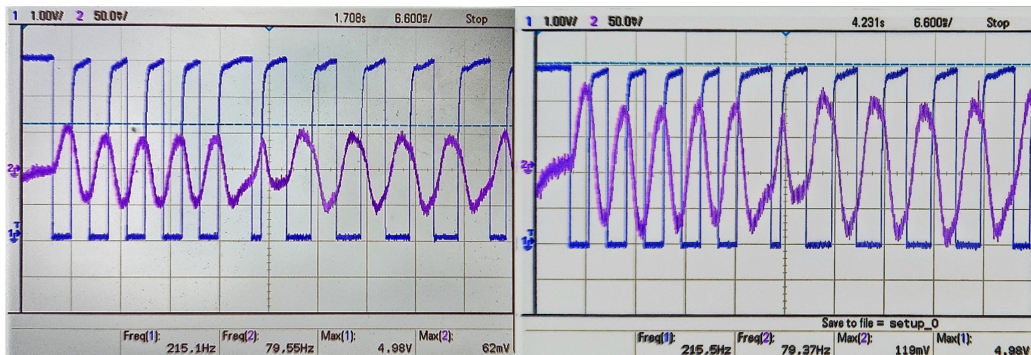


Figure Appendix B.2: Overall setup showing the Communication Subsystem Testing

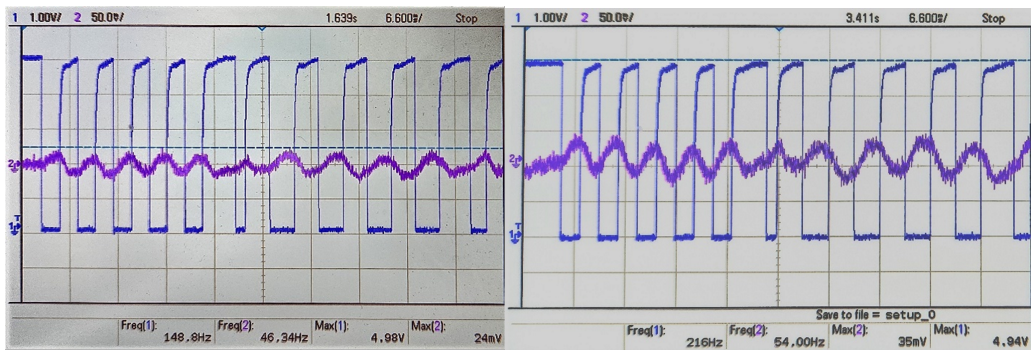
Appendix C. Transmitted Oscilloscope Readings



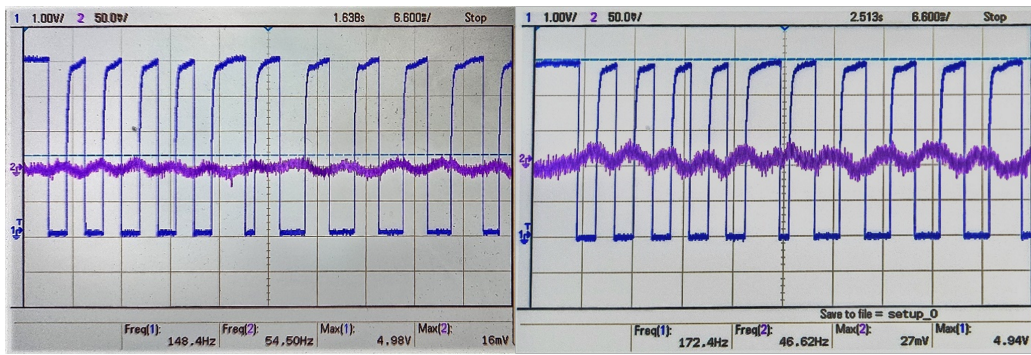
0.2 m — Transmitted and received FSK signals. Left: ambient daylight, Right: dark-room conditions.



0.5 m — Transmitted and received FSK signals. Left: ambient daylight, Right: dark-room conditions.



1.0 m — Transmitted and received FSK signals. Left: ambient daylight, Right: dark-room conditions.



1.5 m — Transmitted and received FSK signals. Left: ambient daylight, Right: dark-room conditions.

Figure Appendix C.1: Transmitted and received FSK signals recorded across four distances under two lighting conditions.